Polymer Crystallization Confined in Hard Spherical Microdomains of Diblock Copolymers

Tao Cai, Yong Qian, Yu Ma, Yijin Ren, and Wenbing Hu*

Department of Polymer Science and Engineering, State Key Laboratory of Coordination Chemistry, School of Chemistry and Chemical Engineering, Nanjing University, 210093 Nanjing, China

Received January 13, 2009; Revised Manuscript Received March 25, 2009

ABSTRACT: We report dynamic Monte Carlo simulations of crystallization under hard confinement of spherical diblock copolymers. We compared the parallel results of blocks with short chains made by breaking block junctions. We observed that blocks crystallize faster but harvest lower crystallinity than short chains, which is in agreement with recent experiments. We found that the fast crystallization can be assigned to the slightly stretched blocks, and the lowered crystallinity is mainly attributed to the frozen block junctions near interfaces. In addition, homogeneous crystal nucleation at low temperatures switches Avrami indexes of both cases from one (first-order kinetics) to 0.5 and meanwhile ruins uniform crystal orientations inside each microdomain. Our present results may facilitate our better understanding of the fabrication of polymer nanocrystals through self-assembly of diblock copolymers.

I. Introduction

It is well known that diblock copolymers can fabricate patterns of nanoscale microdomains through microphase separation at low temperatures.[1,2] Various geometries of microdomains such as lamellae, cylinders, and spheres can be obtained depending mainly on the intramolecular chemical compositions. Such patterns contain many substantial applications as advanced functional materials in microelectronics, device technology, and so on.[3−5] Further crystallization confined in the nanoscale microdomains makes a hierarchical "structure-in-structure" or "order-within-order" morphology.[6,7] There are two typical scenarios of confined crystallization: hard confinement if the glass-transition temperature of the matrix is higher than the crystallization temperature of microdomains, and soft confinement if otherwise.[8] The properties of such-obtained polymer nanocrystals are very much dependent on the structures prepared during crystallization.

Molecular simulations are powerful tools in the study of the crystallization mechanism of polymers under such nanoscale confinement provided by diblock copolymers. By means of dynamic Monte Carlo simulations, the preferences of perpendicular crystal orientations in lamellar microdomains can be attributed to the block junction guiding crystal nucleation at high temperatures.[9] Such preferences are responsible for lamellar undulation and coalescence at high temperatures under soft confinement.[10] A similar story is true in cylindrical microdomains,[11] except for breakdown into a string of small crystallites at high temperatures under soft confinement.[12] For the spherical microdomains, however, their isotropic shapes will not dictate the preferences of crystal orientations over microdomains anymore. Up until now, crystallization confined in the spherical microdomains of diblock copolymers has not yet been investigated by molecular simulations. In this article, along the same approaches of dynamic Monte Carlo simulations, we will address this issue.

Experimental observations on crystallization confined in spherical microdomains of diblock copolymers have been reported by several research groups. Concerning the differences in dimensionality of confinement, it is reasonable to observe the initiation of crystallization confined in spherical microdomains at temperatures lower than those in cylindrical and lamellar microdomains.[13] Loo and his collaborators found that the Avrami index of crystallization appears as one.[14,15] The Avrami index at one reflects first-order kinetics of crystallization contributed by sequential initiation of crystallization in the isolated compartments of spherical microdomains,[14] as evidenced by direct visualization of atomic force microscopy (AFM).[16] Melting of confined small crystallites over a wide temperature range implies that various metastable states are generated.[17] Such first-order kinetics transforms into sigmoidal kinetics upon the occurrence of breakout at high temperatures.[18] AFM observations revealed that the direction of the nearest neighbor of spheres guides the favorite direction of breakout upon crystal growth.[19] However, the crystallinity is substantially decreased with the decrease in spherical-microdomain sizes.[20] Recently, Nojima et al. compared crystallization behaviors between blocks and homopolymers made through photocleavage of blocks, both confined in the similar spherical microdomains.[21] They found a relatively higher crystallinity harvested by homopolymers. Blocks crystallize faster than homopolymers, although both show first-order kinetics upon Avrami analysis.[21] Nevertheless, Lorenzo et al. found that blocks initiate crystallization at temperatures lower than homopolymers confined in the same sizes of droplets,[22] whereas they also observed first-order kinetics for crystallization of blocks.[23,24] Our present simulations will reproduce faster crystallization and lower crystallinity of blocks compared with short chains confined in the same hard spherical microdomains. It will be shown that the faster crystallization can be attributed to a slightly stretched block, and the lower crystallinity can be assigned to the block junctions frozen at interfaces. In addition, the Avrami index switches from first-order kinetics to 0.5 upon synchronization of crystal nucleation over isolated microdomains at low temperatures; meanwhile, crystal orientations lose their uniformity inside each microdomain.

The content of this article is organized as follows. After the Introduction section, the simulation techniques and sample preparation will be briefly introduced, and then the results and discussion are presented. The article ends with a summary of our observations.

II. Simulation Techniques and Sample Preparation

Dynamic Monte Carlo simulations of lattice polymers have been widely applied in the investigations of microscopic

* Corresponding author. E-mail: wbhu@nju.edu.cn.

10.1021/ma900069m CCC: $40.75
Published on Web 04/14/2009

mechanisms of polymer crystallization.[25] The lattice model of polymers assumes that each polymer chain consecutively occupies the lattice sites with one monomer per site. The chain is "living" in the lattice space by performing microrelaxation steps, which allow local sliding diffusion along the chain upon a monomer jumping into its vacancy neighbor with periodic boundary conditions.[25] Bond crossing and double occupation of monomers are forbidden to mimic the excluded-volume interactions of polymers.

In the present simulations, we first prepare spherical microdomains of diblock copolymers by guiding microphase separation from the homogeneous melt and then study crystallization under a hard confinement of glassy matrix. To this end, we put 1920 folded chains, each containing 128 monomers, into a 64^3 cubic lattice. Some vacancy sites are necessary for microrelaxation, playing the role of free volume in the bulk polymer phase. The chains were then relaxed into random-coil states in a homogeneous melt under athermal conditions.

To drive phase separation and crystallization, we employed the conventional Metropolis sampling algorithm with the potential energy barrier

$$E/(kT) = [aE_C + pE_P + bB]/(kT) = [a + pE_P/E_C + bB/E_C]E_C/(kT) \quad (1)$$

where E_C is the bending energy for each pair of bonds consecutively connected along the chain, E_P is the nonparallel packing energy for each pair of parallel neighboring bonds, and B is the mixing energy for each pair of monomers belonging to different species; a, p, and b are the corresponding net pairs in each step of microrelaxation, k is the Boltzmann constant, and T is the temperature. We assumed that in each chain, the first 104 monomers belonged to the noncrystallizable species with a mixing interaction (denoted as parameter B) with the rest of the 24 monomers that were crystallizable species. The crystallizable bonds contain parallel interactions denoted as E_P in the lattice, which has been regarded to be a molecular driving force for polymer crystallization.[25]

In the first step, we simply put the initial homogeneous melt of diblock copolymers under the thermal conditions of $E_P/E_C = 0$, $B/E_C = 0.5$, and the temperature $T = 5E_C/k$. The conditions were chosen for the formation of spherical microdomains according to the phase diagrams obtained in the previous report.[11] After isothermal phase separation for 10^6 MC cycles, where each Monte Carlo (MC) cycle was defined as the number of microrelaxation steps equal to the total amount of lattice sites, the spherical microdomains were spontaneously generated in the sample system, as demonstrated in the snapshot shown in Figure 1. One can see that the spherical microdomains of crystallizable blocks are isolated by the matrix of another species and are roughly arranged in a body-centered cubic structure, implying the achievement of equilibrium microdomains. In total, there are nine spheres, each containing an average of 213 ± 50 crystallizable chains in the cubic box.

In the second step, we supposed that the noncrystallizable matrix is in a glassy state to make a hard confinement to another species. To this end, we simply rejected all microrelaxation steps involving the noncrystallizable monomers. In the following simulations, we fixed the conditions of $E_P/E_C = 1$ and $B/E_C = 0.4$ and set the variable temperatures to observe isothermal crystallization under hard confinement. To expose the role of block junctions, we followed the trick previously employed in both lamellar[9] and cylinder[11] diblock copolymers, cut the block junctions, and compared the parallel crystallization of short 24-mers with that of blocks. After cut, short chains were relaxed for 10^5 MC cycles under athermal conditions to remove the memory of block junctions. This trick has also been played in recent experiments,[21] which offer parallel comparisons of our simulation results with reality.

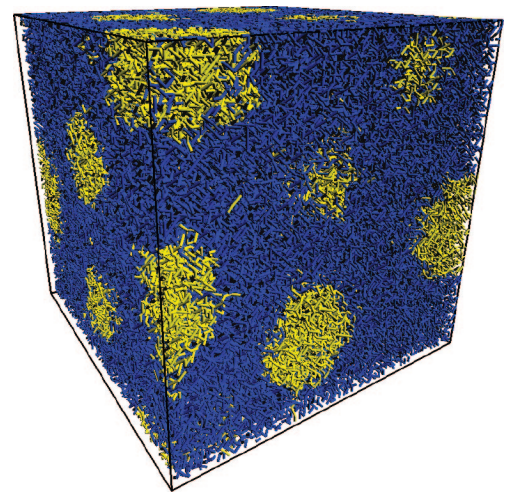

Figure 1. Snapshot of spherical microdomains of diblock copolymers (24:104 of 128-mers in 64^3 cubic lattice box with periodic boundary conditions) prepared by microphase separation under the conditions of $E_P/E_C = 0$, $B/E_C = 0.5$, and temperature $T = 5E_C/k$ after a time period of 10^6 MC cycles. All bonds are drawn in tiny cylinders with the noncrystallizable species in blue and the crystallizable species in yellow.

III. Results and Discussion

Under a specific crystallization temperature, the time (t) evolution of the relative crystallinity (X_c) can be treated by the well-known Avrami equation

$$1 - X_c = \exp(-Kt^n) \quad (2)$$

where the Avrami index, n, characterizes the situation of crystal nucleation and growth, and the kinetic constant, K, reflects the overall crystallization rate.[26] In our simulations, the crystallinity was defined as the fraction of crystallizable bonds containing more than five parallel neighbors of same species.[27] Figure 2a,b summarizes the kinetic constants and the Avrami indexes obtained at various temperatures.

In Figure 2a, under high crystallization temperatures, blocks apparently crystallize faster than short chains. This result is in agreement with the experimental observations of Nojima et al.[21] The reason why blocks can crystallize faster than short chains is worthy of further investigations. Here we looked at the conformation difference between blocks and short chains. Figure 3 compares the radial probability distributions of each free chain end between blocks and short chains within each spherical microdomain. The results are the ensemble statistics of the sample systems at a high temperature without any irreversible crystallization. For the data very close to the domain mass center, they have been raised because of the discrete-lattice effect. One can see a flat plateau for short chains to show the homogeneous density distribution of free chain ends inside microdomains. However, for blocks, their density distribution of free chain ends appears to be higher upon being closer to the domain mass center. Such heterogeneity can be attributed to a stretching of blocks inside each microdomain, whereas the block junctions are fixed at interfaces and the free chain ends are rich around the mass center. Indeed, for the single sample system under the same conditions as those in Figure 3, blocks show the mean square radius of gyration to be 9.99, whereas short chains show it to be 8.27, and blocks show the mean-square end-to-end distance to be 67.15, whereas short chains show it to be 49.65. The large size of blocks indicates their slightly stretching. Such stretching, however, has not been

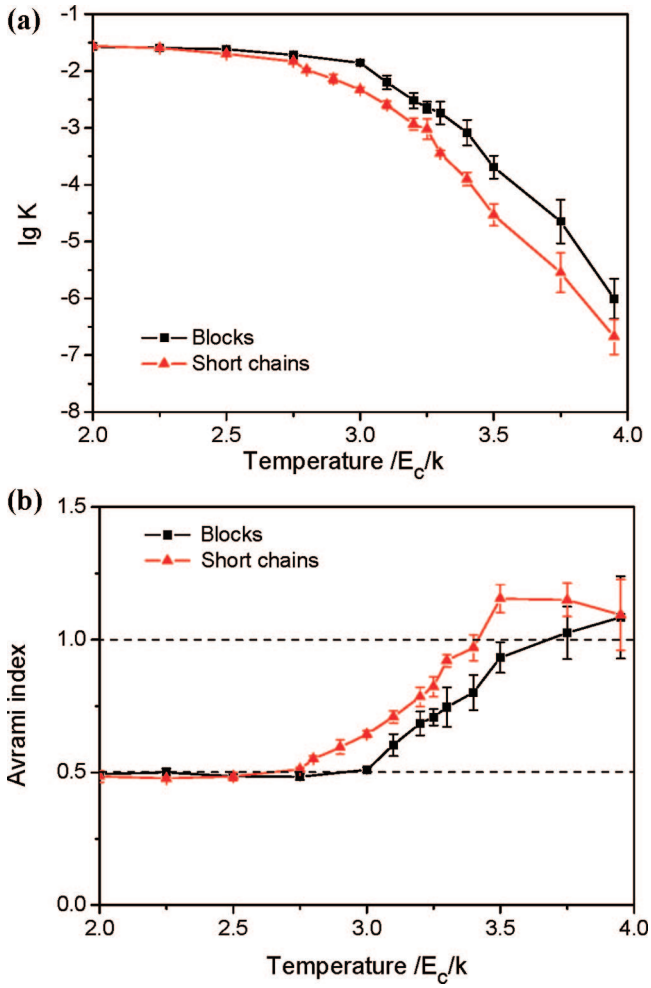

Figure 2. Avrami analysis of isothermal crystallization of blocks and short chains under hard confinement of spherical microdomains at various temperatures with $E_P/E_C = 1$ and $B/E_C = 0.4$: (a) kinetic constants; (b) Avrami indexes. Each reported datum was averaged over five individual processes of the sample systems with different seeds of random-number generation.

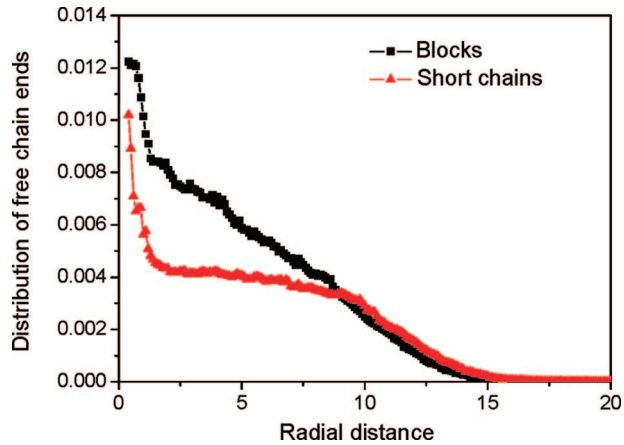

Figure 3. Radial distributions of the probabilities with respect to the center of mass of each spherical microdomain for each free end of blocks and short chains under hard confinement of spherical microdomains at the temperature 4.1 E_C/k with $E_P/E_C = 1$ and $B/E_C = 0.4$. The distribution data were collected over 5000 samples during a long-term evolution with a 200 MC cycles interval and were normalized. We employed the distance defined in continuous space, and the reported data were calculated from each layer of one-tenth of radial distance.

observed under hard confinement of lamellar diblock copolymers.[9] Therefore, the stretching may be associated with an

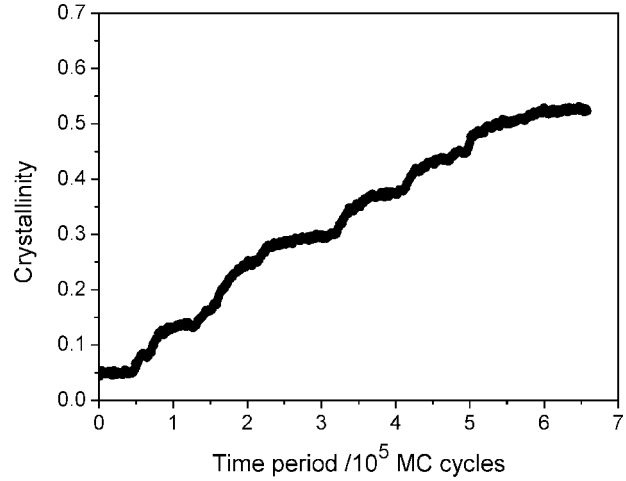

Figure 4. Typical multistep time-evolution curve of overall crystallinity upon isothermal crystallization of blocks under hard confinement of spherical microdomains at $T = 3.95\ E_C/k$ with $E_P/E_C = 1$ and $B/E_C = 0.4$.

overcrowding of blocks tied at the inner side of spherical interfaces with large curvature.

The stretching of blocks will favor the entropy change upon crystallization. Previous simulations have demonstrated that a stretched single chain can induce crystal nucleation to form shish-kebab structures.[28] The similar entropy effect of the block junctions has also been found for crystallization confined in lamellar[9] and cylindrical[11] microdomains, where the perpendicular preferences of crystal orientations result. However, in spherical microdomains, it is obvious that the effect of block junctions (just at the frozen end of blocks) will be much weaker than the effect of stretched blocks (over the whole length of blocks).

Here the blocks and short chains are confined in a glassy compartment made by diblock copolymers, and their surfaces may be quite different from free surfaces with air and flat surface with contacting wall provided by droplets. Deformed polymers contacting the flat surface may facilitate crystal nucleation more than the block junctions. So the initiation of crystallization within droplets can be even faster than the blocks in spherical microdomains.[22] Acceleration in the initiation of polymer crystallization confined in droplets was evidenced by recent molecular simulations.[29]

In Figure 2b, at high temperatures, the Avrami indexes are close to one, implying first-order kinetics of crystallization. As we have already known, the first-order kinetics reflects the sequential initiation of crystallization among microdomains.[14] We indeed observed a typically multistep development of crystallinity upon time evolution of our small sample systems containing a couple of spheres (Figure 1), as shown, for example, in Figure 4. Molecular simulations allow us to perform the Avrami analysis on each isolated sphere. After being averaged over nine spheres, the Avrami index of blocks is 2.098 $\pm$ 0.295 and that of short chains is 2.196 $\pm$ 0.363 at the high temperature 3.95. Such results imply 2D growth of single lamellar crystals with a fixed amount of nuclei at high temperatures. Meanwhile, the kinetic constants, lg K, are -10.68 $\pm$ 0.72 and -11.274 ± 0.415, respectively. Although they are smaller than those shown in Figure 2a for total crystallinity, crystallization rates inside single spheres are still large because of doubled Avrami indexes ($-$lg(t half time) = (lg K $-$ lg(ln 2))/n) and some delay between initiations of crystallization in single spheres. From high to low temperatures in Figure 2b, there exists an apparent transition from first-order kinetics to 0.5. Avrami analysis of single spheres at the low temperature

2.0 gives the same Avrami indexes and kinetic constants as those reported in Figure 2b. Therefore, this transition indicates the fact that when the initiation of primary homogeneous crystal nucleation becomes faster at lower temperatures, the initiation of crystallization among isolated microdomains gradually achieves synchronization. The Avrami index 0.5 has also been reported for crystallization confined in cylindrical microdomains of diblock copolymers.[30] Such a small fractional index implies zero-dimensional initiation of crystallization over isolated microdomains and diffusion-controlled crystallization inside each microdomain.[31] One may imagine that inside each microdomain, the early initiated crystal nuclei may raise a diffusion restriction to the involved chains, and such a restriction will influence all other chains in the microdomain, which makes the later-initiated crystal nuclei appear to be diffusion-controlled. We know that under the diffusion control, the advancing rate of crystal growth front appears as a square root dependence on the reciprocal of time. At low temperatures, crystallization confined in spherical domains may generate a lot of nuclei, but none of them can grow large. Such homogeneous nucleation with zero-dimensional growth may have the Avrami index as one. We suppose that the maturity of nuclei is controlled by 1D crystal growth, and the growth is controlled by diffusion, so the speed of generating nuclei may be proportional to a reciprocal of square root of time; this gives Avrami index 0.5 after the integration with time.

After isothermal crystallization has been saturated for a long term at various temperatures, we estimated the obtained crystallinity. Meanwhile, we also investigated the uniformity of crystal orientations inside each microdomain. Because there is no correlation between two microdomains, the reference axis to calculate the orientational-order parameter of crystalline bonds was chosen as the largest crystallite inside each microdomain. The size of a crystallite was defined by its total amount of bonds containing more than five parallel neighbors. The orientational-order parameter was thus defined as

$$P = <\frac{3\cos^2\theta - 1}{2}> \quad (3)$$

where the angle was for all crystallizable bonds containing more than 10 parallel neighbors of the same species, and <...> was an ensemble average calculated over all spheres in the sample systems. As in the cases of lamellar[9] and cylindrical[11] microdomains, we raised the criteria of parallel neighbors of crystalline bonds from 5 to 10, for a better resolution of the orientational-order parameter. According to the definition in eq 3, when the crystalline bonds exhibit uniform orientations, $P = 1$.

The results for the saturated crystallinities and orientational-order parameters are summarized in Figure 5. One can see that with the increase in temperature, the crystals inside each microdomain show more and more uniform orientations for both blocks and short chains. This tendency is probably related to less crystallites generated inside each microdomain because crystal nucleation becomes a rare event at high temperatures. At high enough temperatures, only one nucleus dominates crystallization inside the microdomain and thus results in uniform orientations of crystalline bonds. Such uniformity is only limited inside each microdomain. Among the spheres, however, the global orientations of crystallites are still random. However, the blocks show less saturated crystallinity than short chains, which is in agreement again with the experimental observations of Nojima et al.[21]

The difference in the saturated crystallinities between blocks and short chains at high temperatures is worthy of further investigation. Therefore, we made visual inspections of the snapshots obtained at high temperatures, as demonstrated, for example, in Figure 6. In comparison with the blocks and short chains in Figure 6, one may recognize that the blocks contain

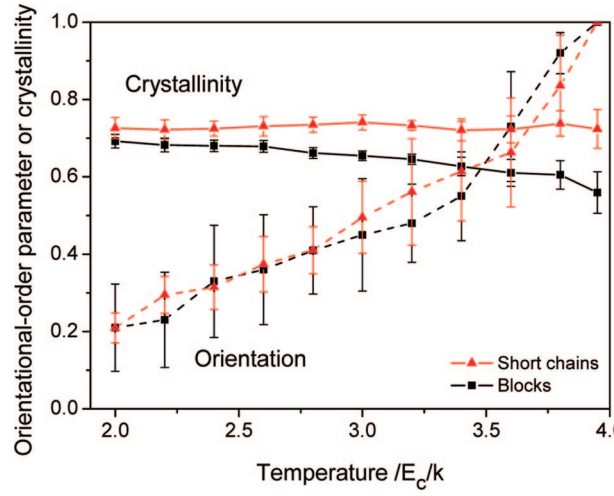

Figure 5. Saturated crystallinities (—) and orientational-order parameters (---) obtained from isothermal crystallization of blocks and short chains under hard confinement of spherical microdomains at various temperatures with $E_P/E_C = 1$ and $B/E_C = 0.4$. The data were collected from 10 individual processes with different seeds of random-number generation.

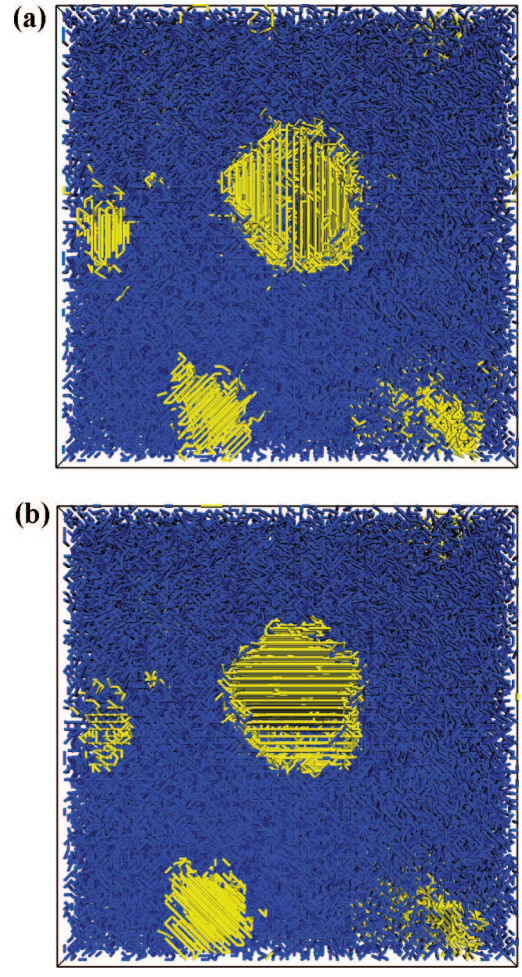

Figure 6. Snapshots of sample systems after saturated isothermal crystallization of (a) blocks and (b) short chains under hard confinement of spherical microdomains at $T = 3.95\ E_C/k$ with $E_P/E_C = 1$ and $B/E_C = 0.4$. All of the bonds are drawn in tiny cylinders with the noncrystallizable species in blue and the crystallizable species in yellow.

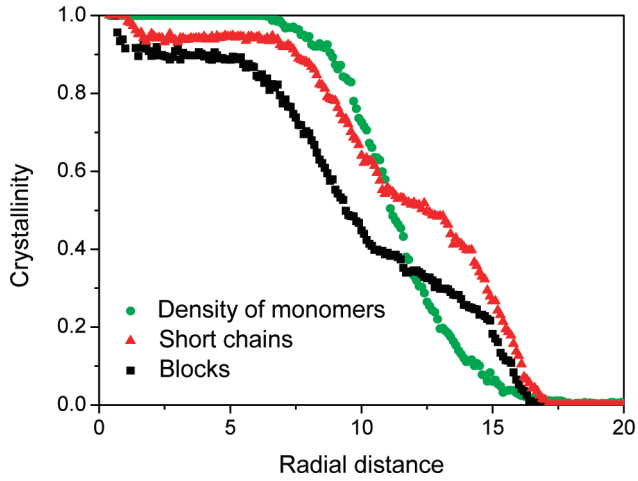

Figure 7. Radial distributions of crystallinities with respect to the center of mass of each spherical microdomain for two sample systems, as denoted after saturated isothermal crystallization under hard confinement of spherical microdomains at $T = 3.95\ E_C/k$ with $E_P/E_C = 1$ and $B/E_C = 0.4$. The radial distribution of monomer density was calculated from the initial state of single spherical microdomains. The data for crystallinities were collected over 50 individual parallel processes of the sample systems with different seeds of random-number generation. We employed the distance in a continuous space, and the reported data were calculated from each layer of one-tenth of the radial distance.

more amorphous fractions near interfaces. Such a low crystallinity near interfaces may be an intrinsic behavior, and it becomes more significant with the decrease in microdomain sizes, leading to a decrease in crystallinity.[20]

Indeed, we made a statistical estimation of radial distributions of crystallinities, as shown in Figure 7. Blocks make less crystallinity mainly near interfaces than short chains. The interfaces at the radial distance can be identified by the radial distribution of monomer densities shown in the same figure. The steplike shoulders on the radial distributions of crystallinities at the outside half of interfaces can be attributed to the anisotropic growth habit of folded-chain lamellar crystal of polymers, which make more amorphous parts of polymers at basal planes (folded-end surfaces) than at lateral surfaces. We know that the only structural difference between the block and a short chain is the block junction. The dominant difference in the distributions of crystallinity near interfaces between two parallel sample systems implies that the block junctions are responsible for the lowered crystallinity near interfaces. One may imagine that the block junctions are frozen at interfaces by the glassy matrix, which will prevent nearby monomers from making necessary reorganization before entering the crystalline phase.

IV. Conclusions

By means of dynamic Monte Carlo simulations, we reproduced experimental observations on polymer crystallization under a hard confinement of spherical microdomain made by diblock copolymers. By comparisons between blocks and short chains under parallel conditions, we learned that blocks are slightly stretched, favoring fast crystallization; however, the block junctions are frozen at interfaces, making lowered crystallinities mainly near interfaces. Upon the occurrence of homogeneous crystal nucleation from high to low temperatures, Avrami indexes switch from first-order kinetics to 0.5, and the orientations of crystalline bonds gradually lose their uniformity inside single microdomains.

Our present results provide another example to demonstrate how molecular simulations can shed light on the microscopic mechanism of polymer crystallization under nanoconfinement. The obtained knowledge may facilitate our better understanding to the fabrication of polymer nanocrystals through self-assembly of diblock copolymers. We have scheduled further investigations under the spherical confinement on how homogeneous nucleation is initiated to make Avrami index 0.5 and how single lamellar crystal grows differently from that in the bulk phase.

Acknowledgment. We acknowledge the financial support from the National Natural Science Foundation of China (NSFC grant nos. 20674036 and 20825415) and the State Key Laboratory for Modification of Chemical Fibers and Polymer Materials at Donghua University of China.

References and Notes

(1) Bates, S.; Fredrickson, G. H. *Annu. Rev. Phys. Chem.* **1990**, *41*, 525.
(2) Bates, S.; Fredrickson, G. H. *Phys. Today* **1999**, *52*, 32.
(3) Park, M.; Harrison, C.; Chaikin, P. M.; Register, R. A.; Adamson, D. H. *Science* **1997**, *276*, 1401.
(4) Cheng, J. Y.; Ross, C. A.; Thomas, E. L.; Smith, H. I.; Vancso, G. *J. Appl. Phys. Lett.* **2002**, *81*, 3657.
(5) Cheng, J. Y.; Mayes, A. M.; Ross, C. A. *Nat. Mater.* **2004**, *3*, 823.
(6) Hamley, I. W. *The Physics of Block Copolymers*; Oxford University Press: Oxford, 1998.
(7) Hamley, I. W. *Adv. Polym. Sci.* **1999**, *148*, 113.
(8) Zhu, L.; Mimnaugh, B. R.; Ge, Q.; Quirk, R. P.; Cheng, S. Z. D.; Thomas, E. L.; Lotz, B.; Hsiao, B. S.; Yeh, F.; Liu, L. *Polymer* **2001**, *42*, 9121.
(9) Hu, W.-B.; Frenkel, D. *Faraday Discuss.* **2005**, *128*, 253.
(10) Hu, W.-B. *Macromolecules* **2005**, *38*, 3977.
(11) Wang, M.-X.; Hu, W.-B.; Ma, Y.; Ma, Y.-Q. *J. Chem. Phys.* **2006**, *124*, 244901.
(12) Qian, Y.; Cai, T.; Hu, W.-B. *Macromolecules* **2008**, *41*, 7625.
(13) Chen, H.-L.; Hsiao, S.-C.; Lin, T.-L.; Yamauchi, K.; Hasegawa, H.; Hashimoto, T. *Macromolecules* **2001**, *34*, 671.
(14) Loo, Y. L.; Register, R. A.; Ryan, A. J. *Phys. Rev. Lett.* **2000**, *84*, 4120.
(15) Loo, Y. L.; Register, R. A.; Ryan, A. J.; Dee, G. T. *Macromolecules* **2001**, *34*, 8968.
(16) Reiter, G.; Castelein, G.; Sommer, J.-U.; Roettele, A.; Thorn-Albrecht, T. *Phys. Rev. Lett.* **2001**, *87*, 226101.
(17) Roettele, A.; Thorn-Albrecht, T.; Sommer, J.-U.; Reiter, G. *Macromolecules* **2003**, *36*, 1257.
(18) Loo, Y. L.; Register, R. A.; Ryan, A. J. *Macromolecules* **2002**, *35*, 2365.
(19) Hobbs, J. K.; Register, R. A. *Macromolecules* **2006**, *39*, 703.
(20) Nojima, S.; Toei, M.; Hara, S.; Tanimoto, S.; Sasaki, S. *Polymer* **2002**, *43*, 4087.
(21) Nojima, S.; Ohguma, Y.; Namiki, S.; Ishizone, T.; Yamaguchi, K. *Macromolecules* **2008**, *41*, 1915.
(22) Lorenzo, A. T.; Arnal, M. L.; Müller, A. J.; Fierro, A. B.; Abetz, V. *Eur. Polym. J.* **2006**, *42*, 516.
(23) Lorenzo, A. T.; Arnal, M. L.; Müller, A. J.; Fierro, A. B.; Abetz, V. *Macromolecules* **2007**, *40*, 5023.
(24) Castillo, R. V.; Arnal, M. L.; Müller, A. J.; Hamley, I. W.; Castelletto, V.; Schmalz, H.; Abetz, V. *Macromolecules* **2008**, *41*, 879.
(25) Hu, W.-B.; Frenkel, D. *Adv. Polym. Sci.* **2005**, *191*, 1, see the appendix.
(26) Avrami, M. *J. Chem. Phys.* **1939**, *7*, 1103.
(27) The possible number of parallel neighbors around each crystallizable bond can be from 0 to 24. We arbitrarily choose the demarcation of five between crystalline and noncrystalline states of the bond. For the details of our lattice model, see the appendix of ref 25.
(28) Hu, W.-B.; Frenkel, D.; Mathot, V. B. F. *Macromolecules* **2002**, *35*, 7172.
(29) Miura, T.; Mikami, M. *Phys. Rev. E* **2007**, *75*, 031804.
(30) Lotz, B.; Kovacs, A. J. *Polym. Prepr. (Am. Chem. Soc., Div. Polym. Chem.)* **1969**, *10*, 820.
(31) Wunderlich, B. Chapter 6.1.3. In *Macromolecular Physics*; Academic Press: New York, 1976; Vol. 2,p 141.

MA900069M